Published in final edited form as:
Neuroimage. 2014 November 15; 102(0 2): 809–816. doi:10.1016/j.neuroimage.2014.08.053.

Lack of dystrophin results in abnormal cerebral diffusion and perfusion *in vivo*

Candida L. Goodnough[a,1], **Ying Gao**[b,c,1], **Xin Li**[c], **Mohammed Q. Qutaish**[c], **L. Henry Goodnough**[d], **Joseph Molter**[b], **David Wilson**[b,c], **Chris A. Flask**[b,c,e], and **Xin Yu**[a,b,c,*]

[a]Department of Physiology and Biophysics, Case Western Reserve University, Cleveland, OH 44106, USA

[b]Department of Radiology, Case Western Reserve University, Cleveland, OH 44106, USA

[c]Department of Biomedical Engineering, Case Western Reserve University, Cleveland, OH 44106, USA

[d]Department of Pathology, Case Western Reserve University, Cleveland, OH 44106, USA

[e]Department of Pediatrics, Case Western Reserve University, Cleveland, OH 44106, USA

Abstract

Dystrophin, the main component of the dystrophin–glycoprotein complex, plays an important role in maintaining the structural integrity of cells. It is also involved in the formation of the blood–brain barrier (BBB). To elucidate the impact of dystrophin disruption *in vivo*, we characterized changes in cerebral perfusion and diffusion in dystrophin-deficient mice (mdx) by magnetic resonance imaging (MRI). Arterial spin labeling (ASL) and diffusion-weighted MRI (DWI) studies were performed on 2-month-old and 10-month-old mdx mice and their age-matched wild-type controls (WT). The imaging results were correlated with Evan's blue extravasation and vascular density studies. The results show that dystrophin disruption significantly decreased the mean cerebral diffusivity in both 2-month-old ($7.38\pm 0.30 \times 10^{-4}$mm^2/s) and 10-month-old ($6.93 \pm 0.53 \times 10^{-4}$ mm^2/s) mdx mice as compared to WT ($8.49\pm0.24\times10^{-4}$, $8.24\pm0.25\times 10^{-4}$mm^2/s, respectively). There was also an 18% decrease in cerebral perfusion in 10-month-old mdx mice as compared to WT, which was associated with enhanced arteriogenesis. The reduction in water diffusivity in mdx mice is likely due to an increase in cerebral edema or the existence of large molecules in the extracellular space from a leaky BBB. The observation of decreased perfusion in the setting of enhanced arteriogenesis may be caused by an increase of intracranial pressure from cerebral edema. This study demonstrates the defects in water handling at the BBB and consequently, abnormal perfusion associated with the absence of dystrophin.

*Corresponding author at: Biomedical Engineering, Radiology, Physiology and Biophysics, Case Western Reserve University, Wickenden 430, 10900 Euclid Avenue, Cleveland, OH 44106. Fax: +1 216 368 4969. xin.yu@case.edu (X. Yu).

[1]These authors contributed equally to this work.

Supplementary data to this article can be found online at http://dx.doi.org/10.1016/j.neuroimage.2014.08.053.

Keywords

dystrophin; perfusion; diffusion; cryoimaging

Introduction

The blood–brain barrier (BBB) ensures the proper physical and metabolic environment for brain function. Endothelial cells lining the vasculature of the brain are joined by tight junctions in order to prevent free diffusion of large and hydrophilic molecules, including water, from the blood into the brain parenchyma (Brightman and Reese, 1969; Reese and Karnovsky, 1967). A major role of the tight junctions is to maintain the physiologic and biochemical environment necessary for neuronal firing. The cytoskeleton is crucial in forming, anchoring, and maintaining the BBB (Zlokovic, 2008). Disruption of the BBB leads to increased permeability of large molecules, such as albumin, into the CNS, causing neuronal dysfunction, edema, and a lower seizure threshold (Abbott et al., 2006; Hawkins and Davis, 2005; Tomkins et al., 2008; van Vliet et al., 2007).

Dystrophin, a major actin-binding component of the dystrophin glycoprotein complex (DGC), links cytoskeletal and membrane elements in the muscle (Tinsley et al., 1994) and brain (Lidov et al., 1990, 1993). Inherited deficiency of functional dystrophin leads to Duchenne muscular dystrophy (DMD), an X-linked recessive disease leading to progressive muscle degeneration. In addition to voluntary muscle weakness, DMD patients suffer from ventilatory and cardiovascular failure at the end stages of the disease. Functional dystrophin is also not expressed in the brains of DMD patients (Hoffman et al., 1987). However, aside from the observation that pediatric DMD patients have lower intelligence quotient (IQ) assessments than that of healthy control children (Cotton et al., 2001; Karagan, 1979), few studies have characterized the structural and functional impact of dystrophin disruption in the brain.

The dystrophin-null *mdx* mouse has been used as a mouse model of muscular dystrophy for over two decades (Sicinski et al., 1989). Aside from the muscular phenotype, cognitive defects have also been observed in *mdx* mice (Vaillend et al., 1995). The tight junction proteins of the BBB were shown to be reduced and dysfunctional in the *mdx* mouse brain, leading to a leaky BBB (Nico et al., 2003). Moreover, enhanced expression of matrix-metalloproteinase (MMP)-2 and -9 in mdx mouse brains was associated with increased expression of vascular endothelial growth factor (VEGF; Nico et al., 2006). These *in vitro* observations provide the evidence of altered brain structure associated with dystrophin deletion. A full understanding of the role of dystrophin in maintaining the BBB and vascularization has yet to be studied *in vivo* with modern imaging technologies which will likely support future clinical investigations.

Arterial spin labeling (ASL) is a non-contrast MRI method that has made significant contributions towards assessing tissue perfusion *in vivo* (Detre et al., 1992; Williams et al., 1992; Edelman et al., 1994; Kwong et al., 1995; Kim and Tsekos, 1997; Wong et al., 1997; Pell et al., 1999; Thomas, 2005). In ASL-MRI, water molecules are “magnetically tagged” in the blood, leading to altered tissue longitudinal magnetization that is proportional to tissue

perfusion. This method does not require exogenous paramagnetic contrast agents as in conventional Dynamic Contrast Enhanced (DCE) MRI perfusion techniques. Hence, ASL-MRI may eventually become the preferred method for longitudinal imaging studies. In spite of its utility, ASL-MRI has yet to be fully applied to understanding the pathophysiologic consequence of dystrophin disruption with regard to water movement and perfusion in the brain.

Diffusion-weighted MRI (DWI) has been invaluable in defining neurological disorders, particularly in the diagnosis of stroke and the assessment of therapeutic interventions (Le Bihan et al., 1986; Kloska et al., 2010; Schellinger et al., 2003; Sevick et al., 1990; Warach et al., 1995). The signal intensity of a DW image reflects the restrictions on Brownian motion of water molecules in the tissue, and the calculated apparent diffusion coefficient (ADC) provides a means to quantify this diffusion under physiologic and pathologic states. High ADC values are characteristic of tissue with relatively free water diffusion, e.g., in extracellular space, as opposed to tissue water with a restricted environment, e.g., in intracellular space (Le Bihan, 2007). Therefore, the diffusion of water molecules as detected by DWI can be used to delineate the neural structure, anatomy, and pathophysiology in the absence of dystrophin.

The goal of this study was to characterize the impact of dystrophin deletion on physiological and structural changes in the brain using both *in vivo* and *in vitro* methods. Cerebral perfusion and brain structure were evaluated by ASL and DWI, respectively. These *in vivo* imaging results were compared with *in vitro* and *ex vivo* studies of vascular density. The present study demonstrates the defects in perfusion and diffusion associated with dystrophin disruption in mdx mice that can be observed *in vivo* with MRI and the association of these *in vivo* imaging assessments with histopathologic measures.

Methods

Animal models

Studies were performed on young (2 months old, $n = 10$) and adult (10 months old, $n = 10$) male dystrophin-null (mdx) and wild-type (WT) mice of the C57/BL6 strain. All mice were obtained from Jackson Laboratories (Bar Harbor, ME). All procedures involving animal care and handling were performed according to institutional guidelines set forth by the Animal Care and Use Committee at Case Western Reserve University.

Perfusion and diffusion MRI

Imaging studies were performed on a 7 T Bruker Biospec (Billerica, MA) horizontal bore MRI scanner. Anesthesia was induced with 2% isoflurane with supplemented O_2 in an isoflurane induction chamber and maintained via nosecone with 1.5% isoflurane once the animal was put in the magnet. The body temperature was monitored and maintained at approximately 36 °C by blowing hot air into the magnet through a feedback control system. Respiratory gating and monitoring was performed through an MR-compatible small animal gating and monitoring system (SA Instruments, Stony Brook, NY) to reduce motion artifacts during image acquisition.

Single-slice axial ASL brain images were acquired with a flow-sensitive alternating inversion recovery (FAIR) preparation sequence followed by a centrically encoded fast imaging in steady precession (FISP) imaging readout (Gao, et al., 2014). Specifically, arterial spin labeling was accomplished by respiratory-triggered, slice-selective (4.5 mm thickness) and non-selective (global) inversion of magnetization, respectively. The inversion pulse used a hyperbolic secant adiabatic inversion pulse with a duration of 3 ms, and the inversion thickness was set to three times that of the excitation pulse to ensure a uniform inversion over the entire imaging slice. An inversion efficiency value of 1 was assumed. The FISP acquisition (including 10 dummy scans) was implemented at 1420 ms following the inversion pulse. This delay time allowed data acquisition to occur during the mid- to late-stage of the subsequent breathing cycle. It is a balance between maximizing blood flow sensitivity and minimizing respiratory motion artifacts. Imaging parameters are: flip angle, 60°; TR, 2.4 ms; TE, 1.2 ms; number of averages, 40; matrix size, 128 × 128; FOV, 30 × 30 mm^2; slice thickness, 1.5 mm. A proton density image (M_0) with no inversion pulse was also acquired using the same imaging parameters. A voxel-wise T_1 map with the same spatial resolution was also acquired with a FISP-based Look-Locker acquisition consisting of a non-selective adiabatic inversion pulse followed by 10 continuous FISP acquisitions with the following parameters: flip angle, 10°; TR, 4.0 ms; TE, 2.0 ms; number of averages, 40. Image reconstruction and analysis were performed offline using custom-built software written in MATLAB (Math Works, Natick, MA). Perfusion maps were generated from the magnetization difference of slice-selective and non-selective inversion images (ΔM), proton density image (M_0), and the T_1 maps (Gao, et al., 2014). A blood/tissue partition coefficient (λ) of 0.9 mL/g was used in this study (Herscovitch and Raichle, 1985).

Single-slice axial diffusion-weighted images (DWI) were acquired with a diffusion-weighted echo-planar imaging (DW-EPI) acquisition. Diffusion weighting was accomplished with two 4-ms (δ) diffusion-encoding gradients separated by 15 ms (Δ), yielding a b value of 500 s/mm^2 applied in the readout direction. The DW-EPI images were acquired with the following parameters: TR, 5000; number of averages, 5; matrix, 128 × 128; FOV, 30 × 30 mm^2; slice thickness, 1 mm. Images were reconstructed and analyzed using custom-built software written in MATLAB (MathWorks, Natick, MA). Voxel-wise apparent diffusion coefficient (ADC) maps were calculated by the established equation: $ADC = \ln(I_0/I)/b$, where I_0 and I are the signal intensity of the b = 0 s/mm^2 and the b = 500 s/mm^2 images, respectively.

Analysis of vascular density by immunocytochemistry

WT (2 mo, n = 4; 10mo, n = 5) and mdx (2 mo, n = 4; 10 mo, n = 5) mice were deeply anesthetized with isoflurane after imaging. The brains were excised and fixed in 4% paraformaldehyde for 24 h at 4 °C. The tissue was transferred to 5% sucrose in PBS for 1 h followed by 20% sucrose overnight at 4 °C. Subsequently, the brains were rapidly frozen in OCT media (Electron Microscopy Sciences, Hatfield, PA) with liquid nitrogen. Tissues were sectioned at 10 μm slice thickness at the location corresponding to the MR imaging slice. A total of 7 sections were obtained from each brain. Indirect immunofluorescence against CD31 (PECAM-1, 1:100; Sigma Aldrich, St. Louis, MO) was performed to assess cerebral vascular density. DAPI (4′,6-diamidino-2-phenylindole dihydrochloride; Sigma

Aldrich, St. Louis, MO) staining was used for nuclear identification. Stained tissue sections were photographed for the DAPI (blue) and PECAM-1 (red) channels. The number of PECAM-1-positive cells per field was quantified. All images were photographed at the same exposure times and magnification. The obtained values from all animals were averaged, and the results were expressed as the mean number of PECAM-1-positive cells per field ± SD.

Analysis of BBB leakage using Evans blue staining

WT (2 months old, $n = 2$; 10 months old, $n = 2$) and mdx (2 months old, $n = 2$; 10 months old, $n = 2$) mice were injected intraperitoneally with a bolus of 0.1 mL/10 g Evans blue (10 mg/mL; Sigma Aldrich, St. Louis, MO). After 24 hours, the mice were deeply anesthetized with isoflurane and the brains were excised and rapidly frozen in OCT media (Electron Microscopy Sciences, Hatfield, PA). Tissues were sectioned at 10 μm slice thickness at the location corresponding to the MR imaging slice. Evans blue extravasation was evaluated by fluorescence in WT versus mdx.

Analysis of vascular density by cryoimaging

The remaining WT (2 months old, $n = 2$; 10 months old, $n = 2$) and mdx (2 months old, $n = 2$, 10months old, $n = 2$) mice were anesthetized with isoflurane and fluorescein isothiocyanate-dextran (FITC-dextran, 10 mg/mL; Sigma Aldrich, St. Louis, MO) was injected intravenously at a dose of 200 mg/kg. After 10 minutes, the brains were excised and rapidly frozen with liquid nitrogen in OCT media (Electron Microscopy Sciences, Hatfield, PA) and mounted to the cryoimaging system. The tissue was sectioned in 25 μm slices and the bright-field and fluorescent images from the cryoimaging system were processed and analyzed with custom-built MATLAB (Mathworks Inc., Natick, MA) and AMIRA (Mercury Computer Systems, San Diego, CA) software (Roy et al., 2009). The brain contour was traced manually from the bright-field images, and a mask was generated. The mask was applied to fluorescent images, and the 3D cerebral vasculature was reconstructed using thresholding and volume rendering methods (Qutaish et al., 2012). The resolution for the reconstructed 3D images were $10.5 \times 10.5 \times 25\ \mu m^3$.

Statistical analysis

All data are reported as mean ± SD. A two-tailed, unpaired Student's *t*-test was performed to compare mdx and WT mice. Statistical significance was established at a level of $p < 0.05$.

Results

Decreased cerebral diffusivity with dystrophin disruption

Representative brain apparent diffusion coefficient (ADC) maps of 2- and 10-month-old mdx and WT mice are shown in Figs. 1a–d. The mean and standard deviation for each group of mice are shown in Fig. 1e. Mean diffusivity in 2-month-old mdx mice was $7.38 \pm 0.30 \times 10^{-4}$ mm^2/s, which was significantly lower than that in age-matched WT mice ($8.49 \pm 0.24 \times 10^{-4}$ mm^2/s; Fig. 1e; $p < 0.0005$). Furthermore, 10-month-old mdx mice also exhibited a decrease in cerebral mean diffusivity as compared to the age-matched WT mice ($6.93 \pm 0.53 \times 10^{-4}$ versus $8.24 \pm 0.25 \times 10^{-4}$ mm^2/s; $p < 0.0005$). In addition, a 2-tailed Student's *t*-test

showed a significant age-related decrease in the mean ADC values of both the WT and mdx mice ($p < 0.05$).

Abnormalities in cerebral perfusion in aged mdx mice

Representative cerebral perfusion maps for the 2- and 10-month-old mdx and WT mice are shown in Figs. 2a–d. The mean and standard deviation for each group are shown in Fig. 2e. There was a 15% decrease in cerebral perfusion in 10-month-old mdx mice as compared to WT (Fig. 2e; $p = 0.001$), without any significant difference in mean cerebral T_1 or M_0 values (p = N.S.). The mean brain perfusion values for the 2-month-old mdx mice were slightly lower than for 2-month-old WT mice. However, no significant difference in cerebral perfusion was observed.

Disruption of blood– brain barrier integrity in mdx mice

To investigate the integrity of the BBB in the absence of dystrophin, we examined the extravasation of Evans blue from blood vessels histologically. There was a significant leakage of Evans blue into the cerebrum of both 2- and 10-month-old mdx mice as demonstrated in Figs. 3a,c. There were few vessels demonstrating Evans blue extravasation in both young (2 months old) and aged (10 months old) WT mouse brains (Figs. 3b,d).

Enhanced cerebral arteriogenesis in aged mdx mice

Representative PECAM-1-stained immunofluorescent images for the 2- and 10-month-old mdx and WT mice are shown in Figs. 4a–d. There was no difference in the amount of cerebral vasculature (number of PECAM-1-positive cells) between the young mdx and WT mice (Fig. 4e). Interestingly, there was enhanced arteriogenesis in the aged (10 months old) mdx mice as compared to the controls, as demonstrated by a 13% increase in PECAM-1-positive cells (Fig. 4e; $p < 0.05$). Representative 3D vessel reconstructions from the FITC-dextran cryoimaging are shown in Fig. 5 (see also Supplemental Videos). Qualitatively, there were more vessels visible in the 2- and 10-month-old mdx mouse brains as compared to WT.

Discussion

In this study, we report the first *in vivo* evaluation of age-dependent alterations in cerebral perfusion and diffusion in mdx mice. In addition to BBB disruption, we have observed increased arteriogenesis in the cerebrum as a result of dystrophin deletion. Traditional Evans blue extravasation confirmed an interruption at the BBB in both the 2- and 10-month-old mdx mice. In addition, *in vivo* DWI experiments established an alteration of the normal cerebral microstructural and physiologic environment in both 2-and 10-month-old mdx mice. Interestingly, decreased *in vivo* perfusion was also present in the 10-month-old mdx mice despite increased arteriogenesis observed in both cryoimaging and immunocytochemistry.

Consistent with the findings by immunocytochemistry, cryoimaging demonstrates extensive arteriogenesis in mdx throughout the entire brain as compared to WT. Previously, enhanced arteriogenesis was observed in the hindlimbs of mdx mice (Straino et al., 2004). It was also

shown that deletion of dystrophin results in enhanced expression of matrix-metalloproteinase (MMP)-2 and -9, which ultimately leads to an increase of VEGF and VEGFR2 expression (Nico et al., 2006). In addition to angiogenesis, increased VEGF activity may also contribute towards an opening of tight junctions at the BBB and enhanced vascular permeability (Schoch et al., 2002; Zhang et al., 2002). The observed increase in arteriogenesis by both cryoimaging and immunocytochemistry in the current study is consistent with the observations of enhanced VEGF activity *in vitro* (Nico et al., 2002). However, unlike the qualitative results from cryoimaging, we did not see a difference in PECAM-1 expression in mdx versus WT mice at 2 months of age. The high-resolution, but limited sampling of the immunofluorescence experiments may better reflect the molecular content of the tissue, whereas the 3D cryoimaging data are more representative of the global macrovascular structure. As such, the global nature of cryoimaging as described herein provides unique and complementary information for these types of investigation.

The decreased cerebral ADC observed in the current study likely represents cellular edema as a result of BBB disruption. BBB disruption in mdx mice due to reduced expression of tight junction proteins has been reported previously (Nico et al., 2003). Consequently, the osmotic influx of water into the cell causes cellular edema and a decrease in extracellular space, leading to a decrease in ADC (Kucharczyk et al., 1991; Moseley et al., 1990). While it has been shown that aqp4 facilitates the clearance of vasogenic edema as a result of BBB disruption (Papadopoulos et al., 2004), the lack of properly functioning aqp4 channels at the BBB in mdx mice (Adams et al., 2008; Frigeri et al., 2001) may prevent the removal of water from the cerebrum and therefore worsen cellular edema. Alternatively, a leaky BBB may also lead to an increase of large molecules in the extracellular space in mdx mice, which may also limit water diffusivity in the extracellular space. Therefore, the observed ADC decrease in mdx brains may be the result of cellular edema, increased extracellular protein content, enhanced vascular permeability, or a combination of these possible mechanisms. The age-dependent reduction of ADC in 10-month-old WT as compared to 2-month-old mice is supported by prior studies, which describe decreasing ADC with age likely due to cellular atrophy and an increase in cerebrospinal fluid (CSF) compartments (Heiland et al., 2002).

To the best of our knowledge, this is the first study that demonstrated decreased perfusion in the setting of increased angiogenesis and a chronically leaky BBB in the mdx brain *in vivo*. This decrease in cerebral perfusion is likely the result of cerebral edema, as observed by DWI. It has been established that the presence of cerebral edema and/or angiogenesis in the fixed volume of the skull leads to an increase in intracranial pressure (ICP; Adams and Ropper, 1997; Mokri, 2001). Increased ICP in this way could decrease cerebral perfusion pressure (CPP), which is the difference between mean arterial pressure and ICP. The control of CPP ensures proper brain function, as a decrease in CPP may lead to ischemia and an increase may contribute towards raising the ICP (Powers, 1991; Schumann et al., 1998). As a result of increased ICP, the consequent decrease of CPP ultimately leads to an autoregulatory decrease in cerebral blood flow. This decrease in perfusion in mdx mice may compromise their ability to react to periods of hypoxia.

There are several limitations in this initial study aimed at investigating whether there were overall changes in diffusion and perfusion in the brain of mdx mice that can be detected by MRI. First, fast imaging sequences were used for both DWI and ASL acquisitions. The voxel size and slice thicknesses used gave rise to partial volume averaging that obscured the small white matter tracts in a mouse brain *in vivo*. Future studies aimed at white/gray matter differentiation/evaluation will require optimization of the imaging parameters or potentially using a different imaging readout approach. Second, instead of performing a comprehensive diffusion tensor imaging study, we performed DWI in order not to overtly extend the acquisition time. While DWI is sensitive to structural changes at the cellular level (e.g., edema), a future diffusion tensor study will be helpful to validate and refine our current findings.

Third, measurement of cerebral perfusion used a single inversion time (TI) and the classic model that assumes equal T_1 for blood and tissue (Detre et al., 1992; Kwong et al., 1995; Kim and Tsekos, 1997). Furthermore, transit time is not considered in the calculation. A more recent model by Pell et al. incorporated both the transit time (δ) and the T_1 of the blood (T_{1a}) and the tissue (T_{1app}) separately (Pell et al., 1999). While the method requires the quantification of both T_{1app} and T_{1a} by using multiple inversion times, it allows more comprehensive assessment of several physiological parameters that can impact blood flow. In calculating the cerebral blood flow (CBF), the classic model and the Pell model used the following equations respectively:

$$\text{Classic:}\mathrm{CBF_C}=\frac{\lambda}{2}\cdot\frac{\Delta M(TI)}{M_0}\cdot\frac{e^{TI/T_1}}{TI}=\frac{\lambda}{2}\cdot\frac{\Delta M(TI)}{M_0}\cdot F_{\mathrm{C}}(T_1,TI)$$

$$\text{Pell:}\mathrm{CBF_P}=\frac{\lambda}{2}\cdot\frac{\Delta M(TI)}{M_0}\cdot e^{\delta/T_{1a}}\cdot\frac{1/T_{1a}-1/T_{1\mathrm{app}}}{e^{-(TI-\delta)/T_{1\mathrm{app}}}-e^{-(TI-\delta)/T_{1a}}}=\frac{\lambda}{2}\cdot\frac{\Delta M(TI)}{M_0}\cdot F_{\mathrm{P}}\left(\delta,T_{1a},T_{1\mathrm{app}},TI\right)$$

where F_C and F_P are the two terms in which the classic model and the Pell model differ. These two terms are defined as:

$$F_{\mathrm{C}}(T_1,TI)=\frac{e^{TI/T_1}}{TI}\quad F_{\mathrm{P}}\left(\delta,T_{1a},T_{1\mathrm{app}},TI\right)=e^{\delta/T_{1a}}\cdot\frac{1/T_{1a}-1/T_{1\mathrm{app}}}{e^{-(TI-\delta)/T_{1\mathrm{app}}}-e^{-(TI-\delta)/T_{1a}}}$$

and T_1 and T_{1app} are related by

$$\frac{1}{T_{1\mathrm{app}}}=\frac{1}{T_1}+\frac{\mathrm{CBF}}{\lambda}$$

Hence, for a measured $\frac{\Delta M(TI)}{M_0}$, the ratio of measured blood flow by the two methods is

$$\frac{\mathrm{CBF_C}}{\mathrm{CBF_P}}=\frac{F_{\mathrm{C}}(T_1,TI)}{F_{\mathrm{P}}\left(\delta,T_{1a},T_{1\mathrm{app}},TI\right)}$$

Using a transit time of 50 ms (Thomas, 2005), a blood T_1 of 2.2 and 2.4 s at 7 T and 9.4 T, respectively (*ex vivo* measurement) (Dobre et al., 2007), and a tissue T_1 of 1.4, 1.6, and 1.8 s, respectively, the simulated differences between the two models with CBF ranging from 100 to 400 mL/min/100 g are shown in Fig. 6. These results suggest that at a field strength of 7 T, the difference between the classic model and the Pell model was <3% when tissue T_1 was 1.8 s. However, the classic model overestimated CBF by 12% to 16% when tissue T_1 was 1.4 s (Figs. 6a and b). In our current study, measured tissue T_1 was ~ 1.7 s. Hence, the calculated CBF difference should be within 8% compared to the Pell model. At 9.4 T, there could be an up to 12% overestimation by the classic model (Figs. 6c and d).

In summary, we have observed abnormal cerebral diffusivity, enhanced angiogenesis, and decreased cerebral perfusion in the mdx mouse. Our study is the first to assess the consequence of dystrophin deletion on cerebral blood flow in the mdx mouse model. *In vivo* mouse studies are essential to further the translational value of these results. Although this work is a step towards clinical translation, better mouse models of DMD need to be studied in further detail since the mdx mouse has a mild phenotype in comparison to the clinical presentation of DMD. The leaky BBB and decreased cerebral perfusion observed in mdx mice may contribute towards the disruption of proper brain function observed in DMD patients. As the life expectancy of DMD patients increases with improved therapies, developing an understanding of the neurologic manifestations of the dystrophin-null phenotype will lead to better patient management when symptoms emerge. In particular, DMD patients suffering from cardiac arrhythmias will be at an increased risk of stroke, and thus understanding dystrophin's role at the BBB and response to hypoxia is critical.

Supplementary Material

Refer to Web version on PubMed Central for supplementary material.

Acknowledgments

The authors would like to acknowledge the support of NIH HL73315 (X. Yu) and AHA 12PRE 12030264 (C.L. Desjardins).

Abbreviations

MRI	magnetic resonance imaging
BBB	blood–brain barrier
DGC	dystrophin–glycoprotein complex
DMD	Duchenne muscular dystrophy
IQ	intelligence quotient
MMP	matrix-metalloproteinase
ASL	arterial spin labeling
DCE	dynamic contrast enhanced

DWI	diffusion-weighted MRI
ADC	apparent diffusion coefficient
mdx	dystrophin-null
FAIR	flow-sensitive alternating inversion recovery
FISP	fast imaging in steady precession
SE	spin-echo
EPI	echo-planar imaging
WT	wild-type
PECAM-1	platelet endothelial cell adhesion molecule
DAPI	4′, 6-diamidino-2-phenylindole dihydrochloride
FITC	fluorescein isothiocyanate
CSF	cerebrospinal fluid
ICP	intracranial pressure
CPP	cerebral perfusion pressure

References

Abbott NJ, Rönnbäck L, Hansson E. Astrocyte–endothelial interactions at the blood–brain barrier. Nat. Rev. Neurosci. 2006; 7:41–53. [PubMed: 16371949]

Adams, R.; Ropper, A. Principles of Neurology. New York: McGraw Hill; 1997.

Adams ME, Tesch Y, Percival JM, Albrecht DE, Conhaim JI, Anderson K, Froehner SC. Differential targeting of nNOS and AQP4 to dystrophin-deficient sarcolemma by membrane-directed alpha-dystrobrevin. J. Cell Sci. 2008; 121:48–54. [PubMed: 18057022]

Brightman MW, Reese TS. Junctions between intimately apposed cell membranes in the vertebrate brain. J. Cell Biol. 1969; 40:648–677. [PubMed: 5765759]

Cotton S, Voudouris NJ, Greenwood KM. Intelligence and Duchenne muscular dystrophy: full-scale, verbal, and performance intelligence quotients. Dev. Med. Child Neurol. 2001; 43:497–501. [PubMed: 11463183]

Detre JA, Leigh JS, Williams DS, Koretsky AP. Perfusion imaging. Magn. Reson. Med. 1992; 23:37–45. [PubMed: 1734182]

Dobre MC, Ugurbil K, Marjanska M. Determination of blood longitudinal relaxation time (T_1) at high magnetic field strengths. Magn. Reson. Imaging. 2007; 25:733–735. [PubMed: 17540286]

Edelman RR, Siewert B, Darby DG, Thangaraj V, Nobre AC, Mesulam MM, Warach S. Qualitative mapping of cerebral blood flow and functional localization with echo-planar MR imaging and signal targeting with alternating radio frequency. Radiology. 1994; 192:513–520. [PubMed: 8029425]

Frigeri A, Nicchia GP, Nico B, Quondamatteo F, Herken R, Roncali L, Svelto M. Aquaporin-4 deficiency in skeletal muscle and brain of dystrophic mdx mice. FASEB J. Off. Publ. Fed. Am. Soc. Exp. Biol. 2001; 15:90–98.

Gao Y, Goodnough CL, Erokwu BO, Farr GW, Darrah R, Lu L, Dell KM, Yu X, Flask CA. Arterial spin labeling-fast imaging with steady- state free precession (ASL-FISP): a rapid and quantitative perfusion technique for high-field MRI. NMR Biomed. 2014 http://dx.doi.org/10.1002/nbm.3143 (Epub ahead of print).

Hawkins BT, Davis TP. The blood–brain barrier/neurovascular unit in health and disease. Pharmacol. Rev. 2005; 57:173–185. [PubMed: 15914466]

Heiland S, Sartor K, Martin E, Bardenheuer HJ, Plaschke K. *In vivo* monitoring of age-related changes in rat brain using quantitative diffusion magnetic resonance imaging and magnetic resonance relaxometry. Neurosci. Lett. 2002; 334:157–160. [PubMed: 12453619]

Herscovitch P, Raichle ME. What is the correct value for the brain–blood partition coefficient for water? J. Cereb. Blood Flow Metab. 1985; 5:65–69. [PubMed: 3871783]

Hoffman EP, Brown RH Jr, Kunkel LM. Dystrophin: the protein product of the Duchenne muscular dystrophy locus. Cell. 1987; 51:919–928. [PubMed: 3319190]

Karagan NJ. Intellectual functioning in Duchenne muscular dystrophy: a review. Psychol. Bull. 1979; 86:250–259. [PubMed: 382221]

Kim SG, Tsekos NV. Perfusion imaging by a flow-sensitive alternating inversion recovery (FAIR) technique: application to functional brain imaging. Magn. Reson. Med. 1997; 37:425–435. [PubMed: 9055234]

Kloska SP, Wintermark M, Engelhorn T, Fiebach JB. Acute stroke magnetic resonance imaging: current status and future perspective. Neuroradiology. 2010; 52:189–201. [PubMed: 19967531]

Kucharczyk J, Mintorovitch J, Asgari H, Tsuura M, Moseley M. *In vivo* diffusion-perfusion magnetic resonance imaging of acute cerebral ischemia. Can. J. Physiol. Pharmacol. 1991; 69:1719–1725. [PubMed: 1804517]

Kwong KK, Chesler DA, Weisskoff RM, Donahue KM, Davis TL, Ostergaard L, Campbell TA, Rosen BR. MR perfusion studies with T1-weighted echo planar imaging. Magn. Reson. Med. 1995; 34:878–887. [PubMed: 8598815]

Le Bihan D. The ‘wet mind’: water and functional neuroimaging. Phys. Med. Biol. 2007; 52:R57–R90. [PubMed: 17374909]

Le Bihan D, Breton E, Lallemand D, Grenier P, Cabanis E, Laval-Jeantet M. MR imaging of intravoxel incoherent motions: application to diffusion and perfusion in neurologic disorders. Radiology. 1986; 161:401–407. [PubMed: 3763909]

Lidov HGW, Byers TJ, Watkins SC, Kunkel LM. Localization of dystrophin to postsynaptic regions of central nervous system cortical neurons. Nature. 1990; 348:725–728. [PubMed: 2259381]

Lidov HGW, Byers TJ, Kunkel LM. The distribution of dystrophin in the murine central nervous system: an immunocytochemical study. Neuroscience. 1993; 54:167–187. [PubMed: 8515841]

Mokri B. The Monro–Kellie hypothesis. Applications in CSF volume depletion. Neurology. 2001; 56:1746–1748. [PubMed: 11425944]

Moseley ME, Cohen Y, Mintorovitch J, Chileuitt L, Shimizu H, Kucharczyk J, Wendland MF, Weinstein PR. Early detection of regional cerebral ischemia in cats: comparison of diffusion- and T2-weighted MRI and spectroscopy. Magn. Reson. Med. 1990; 14:330–346. [PubMed: 2345513]

Nico B, Corsi P, Vacca A, Roncali L, Ribatti D. Vascular endothelial growth factor and vascular endothelial growth factor receptor-2 expression in mdx mouse brain. Brain Res. 2002; 953:12–16. [PubMed: 12384233]

Nico B, Frigeri A, Nicchia GP, Corsi P, Ribatti D, Quondamatteo F, Herken R, Girolamo F, Marzullo A, Svelto M, et al. Severe alterations of endothelial and glial cells in the blood–brain barrier of dystrophic mdx mice. Glia. 2003; 42:235–251. [PubMed: 12673830]

Nico B, Corsi P, Ria R, Crivellato E, Vacca A, Roccaro AM, Mangieri D, Ribatti D, Roncali L. Increased matrix-metalloproteinase-2 and matrix-metalloproteinase-9 expression in the brain of dystrophic mdx mouse. Neuroscience. 2006; 140:835–848. [PubMed: 16650610]

Papadopoulos MC, Manley GT, Krishna S, Verkman AS. Aquaporin-4 facilitates reabsorption of excess fluid in vasogenic brain edema. FASEB J. Off. Publ. Fed. Am. Soc. Exp. Biol. 2004; 18:1291–1293.

Pell GS, Thomas David L, Lythgoe MF, Fernando Calamante F, Howseman AM, Gadian DG, Ordidge RJ. Implementation of quantitative FAIR perfusion imaging with a short repetition time in time-course studies. Magn. Reson. Med. 1999; 41:829–840. [PubMed: 10332861]

Powers WJ. Cerebral hemodynamics in ischemic cerebrovascular disease. Ann. Neurol. 1991; 29:231–240. [PubMed: 2042939]

Qutaish MQ, Sullivant KE, Burden-Gulley SM, Lu H, Roy D, Wang J, Basilion JP, Brady-Kalnay SM, Wilson DL. Cryo-image analysis of tumor cell migration, invasion, and dispersal in a mouse xenograft model of human glioblastoma multiforme. Mol. Imaging Biol. MIB Off. Publ. Acad. Mol. Imaging. 2012; 14:572–583.

Reese TS, Karnovsky MJ. Fine structural localization of a blood–brain barrier to exogenous peroxidase. J. Cell Biol. 1967; 34:207–217. [PubMed: 6033532]

Roy D, Steyer GJ, Gargesha M, Stone ME, Wilson DL. 3D cryo-imaging: a very high-resolution view of the whole mouse. Anat. Rec. Hoboken NJ 2007. 2009; 292:342–351.

Schellinger PD, Fiebach JB, Hacke W. Imaging-based decision making in thrombolytic therapy for ischemic stroke: present status. Stroke J. Cereb. Circ. 2003; 34:575–583.

Schoch HJ, Fischer S, Marti HH. Hypoxia-induced vascular endothelial growth factor expression causes vascular leakage in the brain. Brain. 2002; 125:2549–2557. [PubMed: 12390979]

Schumann P, Touzani O, Young AR, Morello R, Baron JC, MacKenzie ET. Evaluation of the ratio of cerebral blood flow to cerebral blood volume as an index of local cerebral perfusion pressure. Brain J. Neurol. 1998; 121(Pt 7):1369–1379.

Sevick RJ, Kucharczyk J, Mintorovitch J, Moseley ME, Derugin N, Norman D. Diffusion-weighted MR imaging and T2-weighted MR imaging in acute cerebral ischaemia: comparison and correlation with histopathology. Acta Neurochir. Suppl. (Wien). 1990; 51:210–212. [PubMed: 1708645]

Sicinski P, Geng Y, Ryder-Cook AS, Barnard EA, Darlison MG, Barnard PJ. The molecular basis of muscular dystrophy in the mdx mouse: a point mutation. Science. 1989; 244:1578–1580. [PubMed: 2662404]

Straino S, Germani A, Di Carlo A, Porcelli D, De Mori R, Mangoni A, Napolitano M, Martelli F, Biglioli P, Capogrossi MC. Enhanced arteriogenesis and wound repair in dystrophin-deficient mdx mice. Circulation. 2004; 110:3341–3348. [PubMed: 15545520]

Thomas DL. Arterial spin labeling in small animals: methods and applications to experimental cerebral ischemia. 2005

Tinsley JM, Blake DJ, Zuellig RA, Davies KE. Increasing complexity of the dystrophin-associated protein complex. Proc. Natl. Acad. Sci. 1994; 91:8307–8313. [PubMed: 8078878]

Tomkins O, Shelef I, Kaizerman I, Eliushin A, Afawi Z, Misk A, Gidon M, Cohen A, Zumsteg D, Friedman A. Blood–brain barrier disruption in post-traumatic epilepsy. J. Neurol. Neurosurg. Psychiatry. 2008; 79:774–777. [PubMed: 17991703]

Vaillend C, Rendon A, Misslin R, Ungerer A. Influence of dystrophin-gene mutation on mdx mouse behaviour. I. Retention deficits at long delays in spontaneous alternation and bar-pressing tasks. Behav. Genet. 1995; 25:569–579. [PubMed: 8540895]

Van Vliet EA, da Costa Araújo S, Redeker S, van Schaik R, Aronica E, Gorter JA. Blood–brain barrier leakage may lead to progression of temporal lobe epilepsy. Brain. J. Neurol. 2007; 130:521–534.

Warach S, Gaa J, Siewert B, Wielopolski P, Edelman RR. Acute human stroke studied by whole brain echo planar diffusion-weighted magnetic resonance imaging. Ann. Neurol. 1995; 37:231–241. [PubMed: 7847864]

Williams DS, Detre JA, Leigh JS, Koretsky AP. Magnetic resonance imaging of perfusion using spin inversion of arterial water. Proc. Natl. Acad. Sci. U. S. A. 1992; 89:212–216. [PubMed: 1729691]

Wong EC, Buxton RB, Frank LR. Implementation of quantitative perfusion imaging techniques for functional brain mapping using pulsed arterial spin labeling. NMR Biomed. 1997; 10:237–249. [PubMed: 9430354]

Zhang ZG, Zhang L, Tsang W, Soltanian-Zadeh H, Morris D, Zhang R, Goussev A, Powers C, Yeich T, Chopp M. Correlation of VEGF and angiopoietin expression with disruption of blood–brain barrier and angiogenesis after focal cerebral ischemia. J. Cereb. Blood Flow Metab. Off. J. Int. Soc. Cereb. Blood Flow Metab. 2002; 22:379–392.

Zlokovic BV. The blood–brain barrier in health and chronic neurodegenerative disorders. Neuron. 2008; 57:178–201. [PubMed: 18215617]

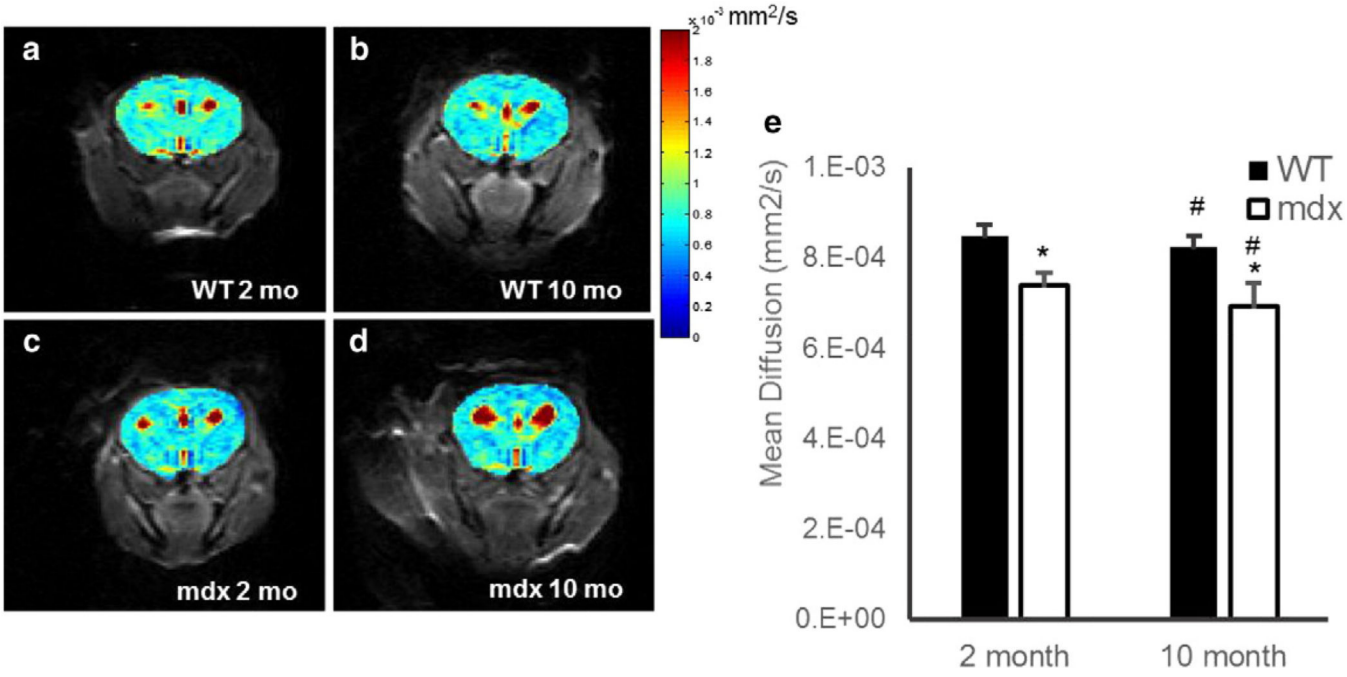

Fig. 1.

a–d. Representative diffusion images of 2-month-old WT (a), 2-month-old mdx (b), 10-month-old WT (c), and 10-month-old mdx (d). e. Mean cerebral (excluding ventricles) diffusion in C57/BL6 WT (black) and mdx (white), respectively. There was a significant decrease in mean diffusion as compared to WT observed in the mdx in both the 2- and 10-month-old mice (*$p < 0.0005$). There was also a significant age-dependent decrease in diffusion in young versus aged WT and mdx mice, respectively (#$p < 0.05$). Data represented as mean ± SD. Color bar is uniform in each panel.

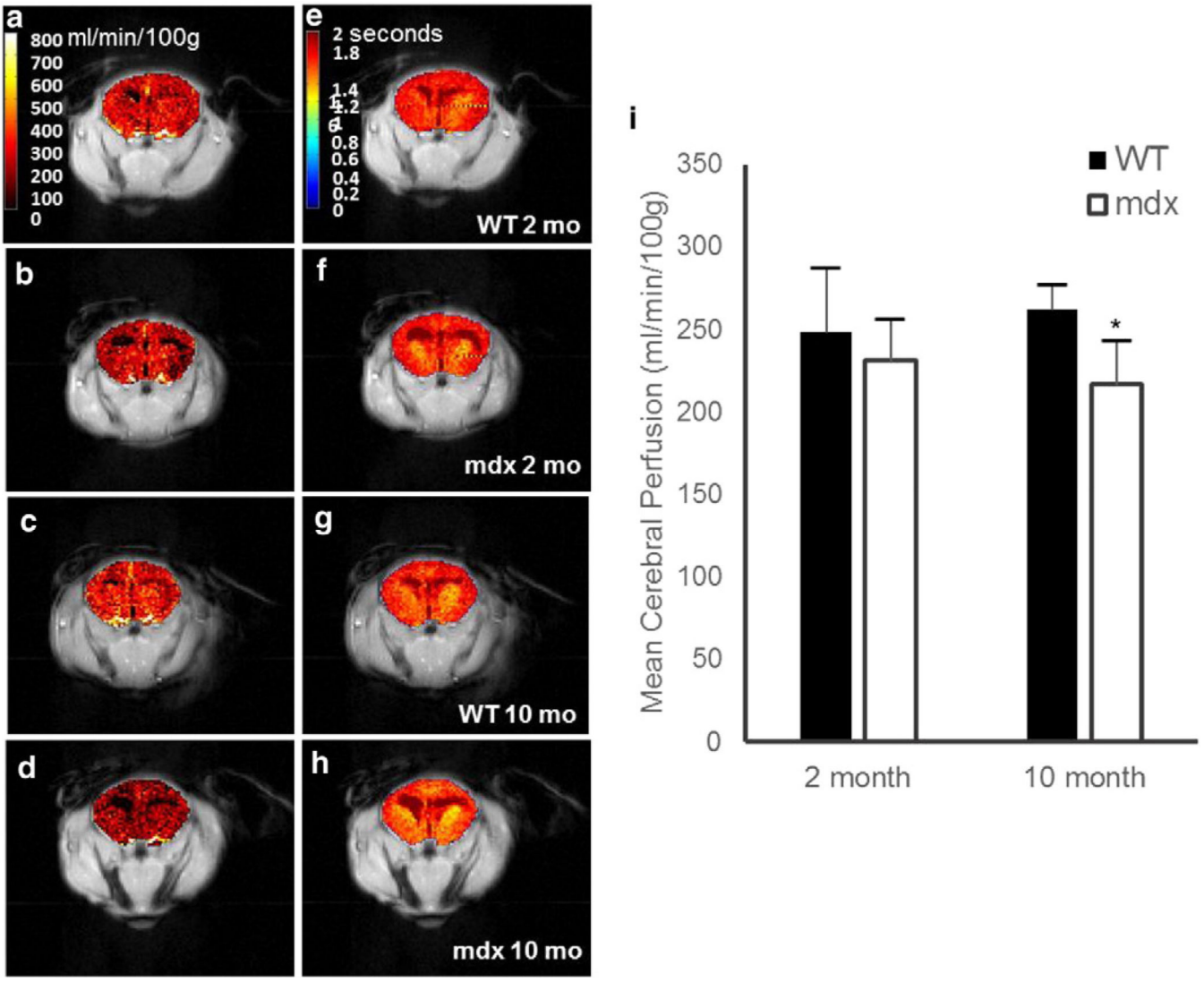

Fig. 2.

a–d. Representative perfusion images of 2-month-old WT (a), 2-month-old mdx (b), 10-month-old WT (c), and 10-month-old mdx (d). e–h. Representative T_1 maps of 2-month-old WT (e), 2-month-old mdx (f), 10-month-old WT (g), and 10-month-old mdx (h). i. Mean cerebral (excluding ventricles) perfusion from the ASL-FISP method in C57/BL6 WT (black) and mdx (white), respectively. There was a significant decrease in mean perfusion as compared to aged WT observed in the aged mdx mice ($p < 0.005$). There was no significant change in perfusion in young versus aged WT ($p > 0.3$) or young versus aged mdx ($p > 0.3$), respectively. Data represented as mean ± SD. Color bar is uniform in each panel.

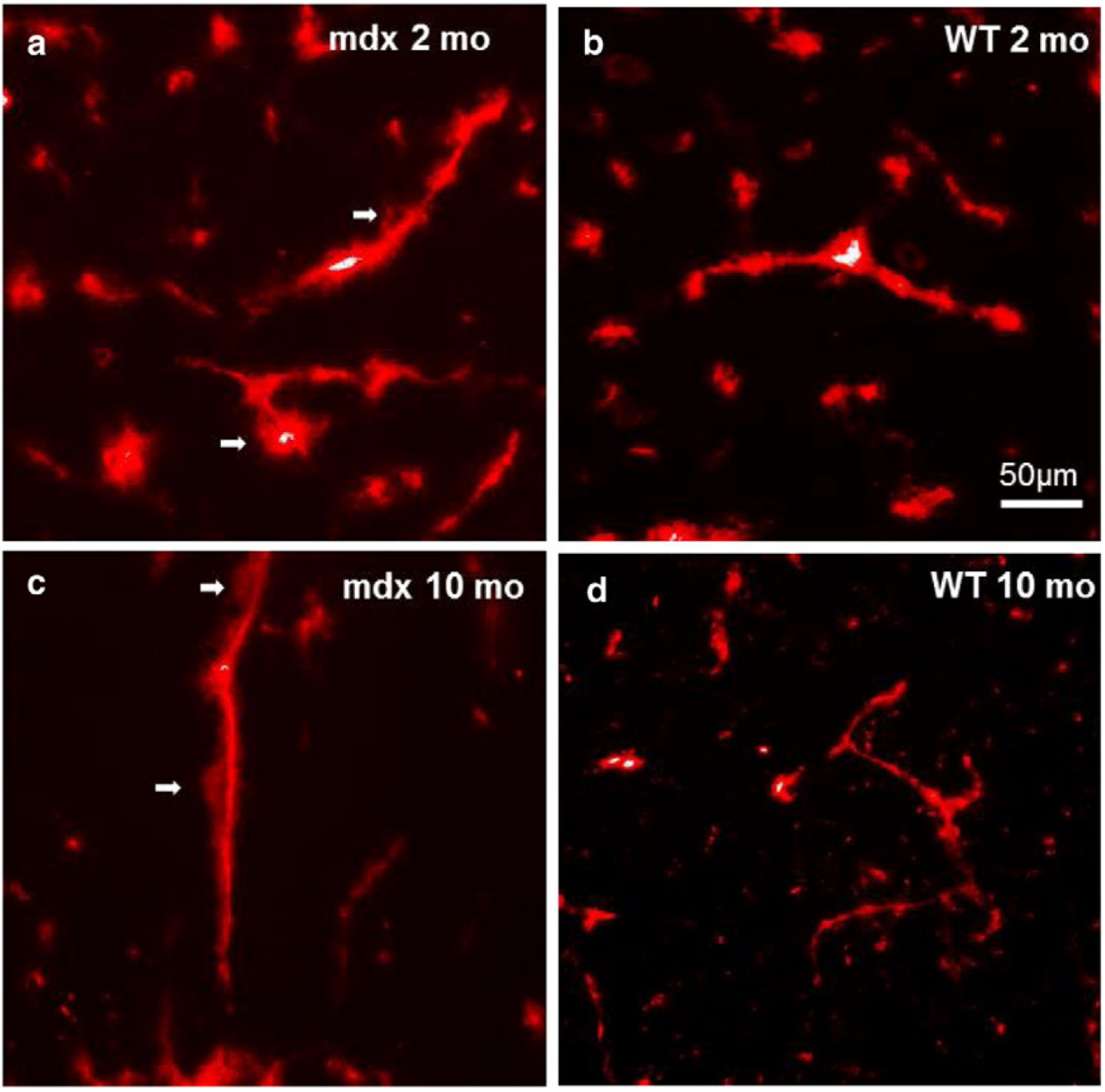

Fig. 3.

a–d. Representative images of Evan's blue fluorescence on axial sections of frozen 2-month-old mdx (a), 2-month-old WT (b), 10-month-old mdx (c), and 10-month-old WT (d). Note the extravasation of Evan's blue (arrows) in the mdx mice.

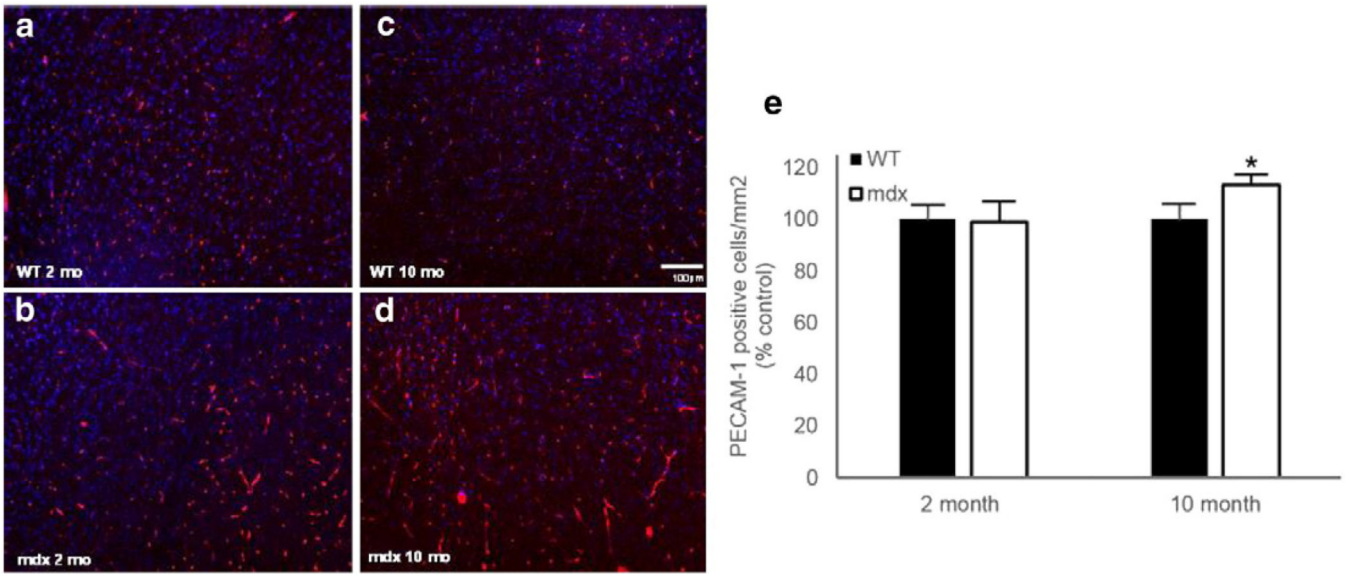

Fig. 4.

a–d. Representative images of indirect immunofluorescence against CD31 (platelet endothelial cell adhesion molecule 1, PECAM-1) on axial sections of paraformaldehyde-fixed frozen 2-month-old WT (a), 2-month-old mdx (b), 10-month-old WT (c), and 10-month-old mdx (d). e. Quantification of PECAM-1-positive cells in 2- and 10-month-old mdx and WT mice. Data are represented as mean ± SD. *$p < 0.05$ versus WT.

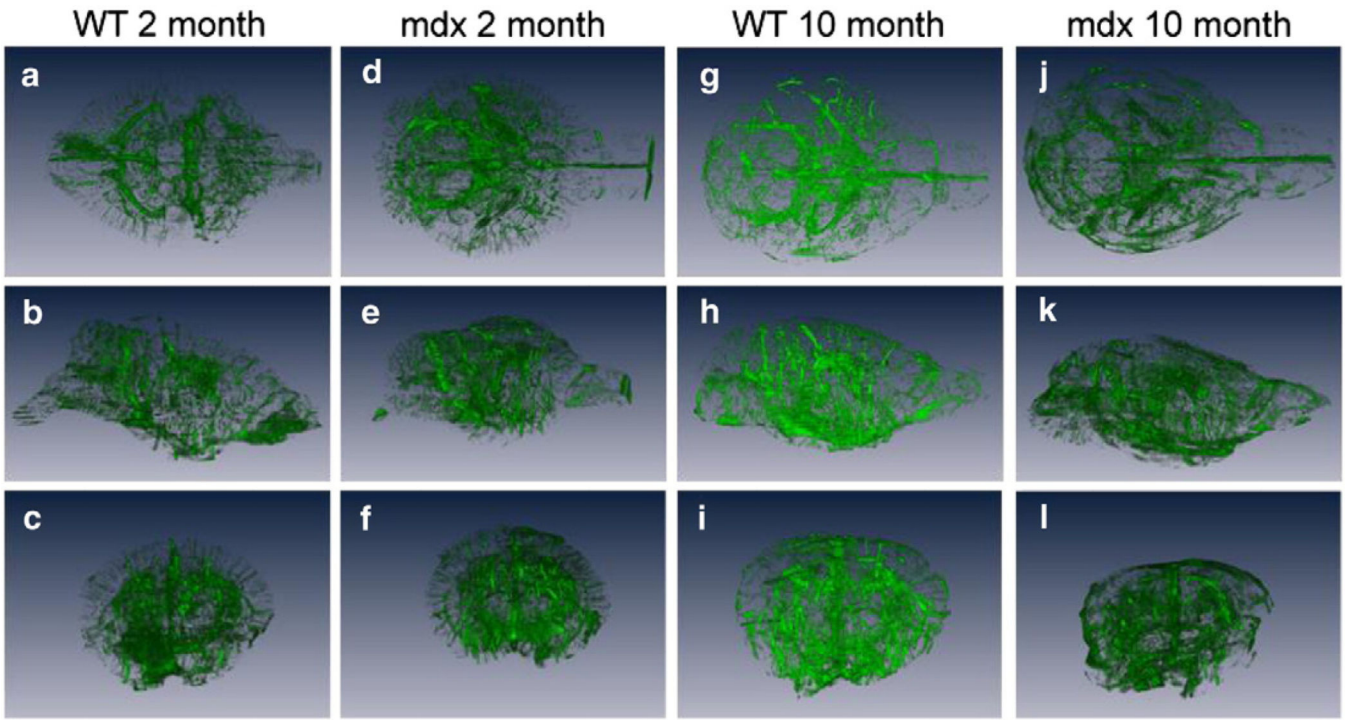

Fig. 5.

a–l. Representative dorsal (top row), lateral (middle row), and (bottom row) views of the 3D vessel reconstructions from 2-month-old WT (a–c), 2-month-old mdx (d–f), 10-month-old WT (g–i), and 10-month-old mdx (j–l).

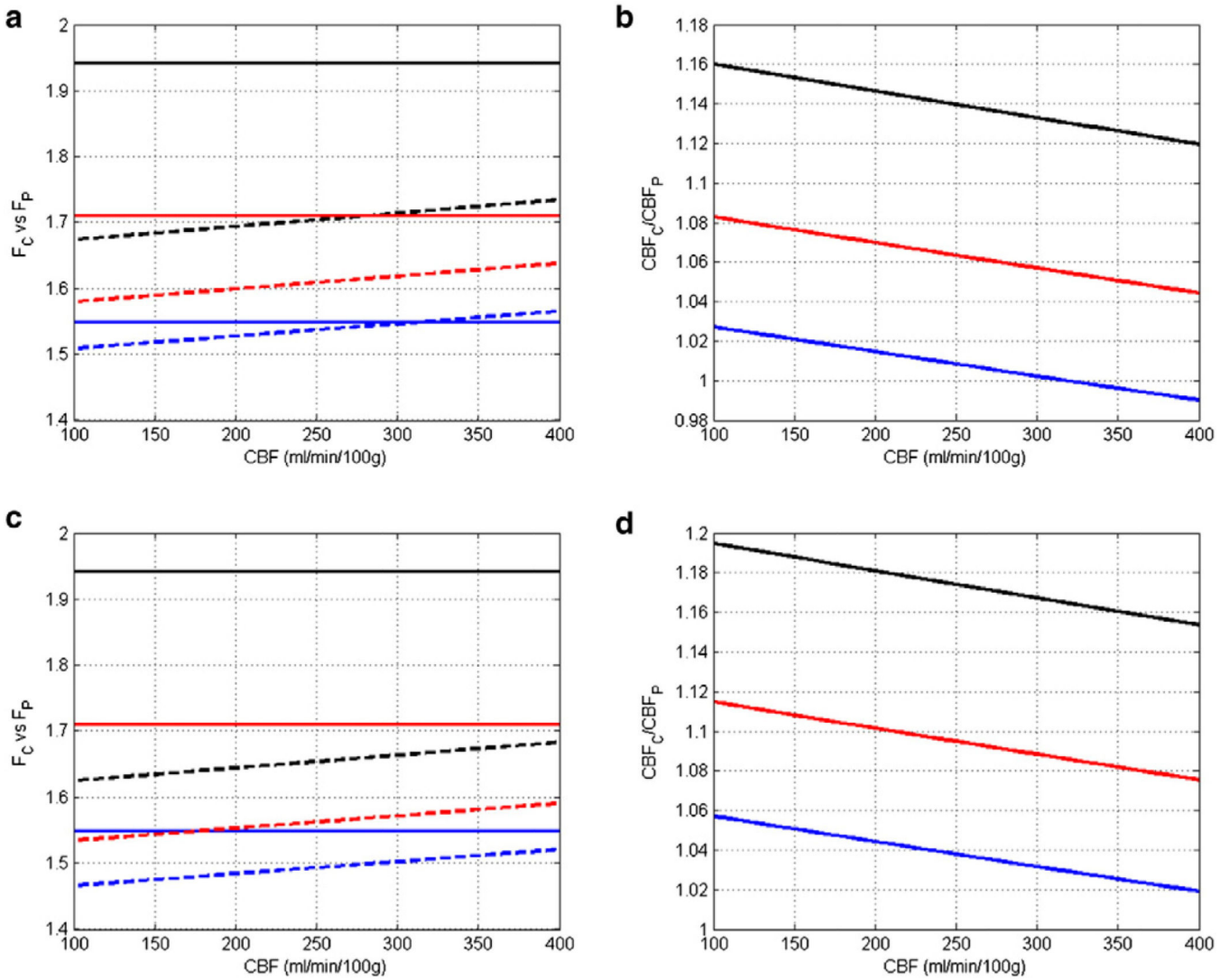

Fig. 6.

Comparison of the classic model and the Pell model. a and b. Simulated F_c and F_p, and CBF_c/CBF_P at 7 T, respectively. c and d. Simulated F_c and F_p, and CBF_c/CBF_P at 9.4 T, respectively. Solid lines in a and c represent the classic model, while dotted lines represent the Pell model. Black, red, and blue represent tissue T_1 of 1.4, 1.6, and 1.8 s, respectively.